Mitochondrial fission is associated with UCP1 activity in human brite/beige adipocytes

Didier Pisani, Valentin Barquissau, Jean-Claude Chambard, Diane Beuzelin, Rayane Ghandour, Maude Giroud, Aline Mairal, Sophie Pagnotta, Saverio Cinti, Dominique Langin, et al.

Mitochondrial fission is associated with UCP1 activity in human brite/beige adipocytes

Didier F Pisani[1,+*], Valentin Barquissau[2,3,+], Jean-Claude Chambard[1], Diane Beuzelin[2,3], Rayane A Ghandour[1], Maude Giroud[1], Aline Mairal[2,3], Sophie Pagnotta[1,4], Saverio Cinti[5,6], Dominique Langin[2,3,7] and Ez-Zoubir Amri[1*]

[1] Université Côte d'Azur, CNRS, Inserm, iBV, Nice, France.
[2]Inserm, UMR1048, Obesity Research Laboratory, Institute of Metabolic and Cardiovascular Diseases, Toulouse, 31432, France
[3]University of Toulouse, UMR1048, Paul Sabatier University, Toulouse, 31432, France
[4]Centre Commun de Microscopie Appliquée, Microscopy and Imaging platform Côte d'Azur, Nice, 06108, France
[5]Department of Experimental and Clinical Medicine, University of Ancona (Politecnica Delle Marche), Ancona, 60121, Italy
[6]Center of Obesity, University of Ancona (Politecnica Delle Marche)–United Hospitals, Ancona, 60121, Italy
[7]Toulouse University Hospitals, Department of Clinical Biochemistry, Toulouse, 31059, France
*Corresponding authors: Didier Pisani : pisani@unice.fr; Ez-Zoubir Amri : amri@unice.fr
Institut de Biologie Valrose, Univ. Nice Sophia Antipolis, 28, avenue de Valombrose, 06107 Nice Cedex 2, France. Tel: +33 493 37 70 82; Fax: +33 493 81 70 58
[+] These authors equally contributed to this work

Abstract

Objective

Thermogenic adipocytes (*i.e.* brown or brite/beige adipocytes) are able to burn large amounts of lipids and carbohydrates as a result of highly active mitochondria and enhanced uncoupled respiration, due to UCP1 activity. Although mitochondria are the key organelles for this thermogenic function, limited human data are available.

Methods/results

We characterized changes in the mitochondrial function of human brite adipocytes, using hMADS cells as a model of white- to brite-adipocyte conversion. We found that profound molecular modifications were associated with morphological changes in mitochondria. The fission process was partly driven by the DRP1 protein, which also promoted mitochondrial uncoupling.

Conclusion

Our data demonstrate that white-to-brite conversion of human adipocytes relies on molecular, morphological and functional changes in mitochondria, which enable brite/beige cells to carry out thermogenesis.

Keywords

hMADS, UCP1, DRP1, brite/beige adipocyte, mitochondria.

1. Introduction

Overweight and obesity are a consequence of an energy imbalance, which leads to an increase in white fat mass. Brown adipocytes and their activation are promising targets for the treatment of human obesity [1, 2], because these cells show high metabolic activity under stimulated conditions in both rodents and adult humans [3-7]. Thermogenic adipocytes are found in discrete brown adipose tissue (BAT) depots as brown adipocytes and are interspersed in white fat depots as ‘brite/beige' adipocytes [8, 9]. Depending on their anatomical location, thermogenic adipocytes found in humans display a molecular signature of either classical brown or brite/beige fat cells [10-17].

Given the abundance of white adipose tissue (WAT) in humans, there is growing clinical interest in understanding how brite adipocytes develop, especially since their emergence has been associated with protection against obesity and metabolic dysfunctions in rodents [18-21]. Brite adipocytes are derived either from progenitors, or for a large proportion of cells, through direct conversion of mature white adipocytes [22-24]. This mechanism of conversion highlights the plasticity of adipocytes in response to specific physiological situations [25, 26]. Compared to white adipocytes, brown and brite adipocytes possess a higher mitochondrial content and express the uncoupling protein 1 (UCP1), which facilitates a proton leak and the uncoupling of the respiratory chain [27, 28]. This phenomenon results in a high oxidative capacity and increased energy expenditure, which leads to thermogenesis. Conversely, white adipocytes contain fewer mitochondria but their function is essential for adipocyte differentiation and function [29]. Mitochondria are dynamic organelles that display morphological changes, such as fusion/fission events, which represent an adaptation to the needs of the cell [30]. The increased mass of mitochondria, important for brown adipocyte function, and involves a coordinated interaction between the nuclear and mitochondrial genomes. Mitochondria continuously undergo fusion and fission events: conditions requiring high mitochondrial ATP synthesis are associated with mitochondrial elongation [30, 31], whereas, bioenergetic stress induces mitochondrial

fragmentation, which may lead to apoptosis [30, 32]. However, mitochondrial fission may not be deleterious *per se* in brown adipocytes. Indeed, adrenergic stimulation of rodent brown adipocytes induces substantial changes in the mitochondrial architecture, including a high rate of fragmentation [33, 34]. This phenomenon favors enhanced mitochondrial uncoupling and energy expenditure. Taken together, these observations highlight the importance of mitochondrial biogenesis and dynamics in the function of brite and brown adipocytes.

The *in vivo* discrepancies between mice and humans in terms of the amount and location of brite fat cells, as well as the difficulty in routinely obtaining fresh human samples, underline the need to decipher the mechanisms regulating brite adipocyte formation and activity in human cells [35]. Herein, we have characterized the properties of the mitochondria during the conversion of human white to brite adipocytes using the human Multipotent Adipose Derived Stem Cell (hMADS) model [36]. We found that human brite adipocyte mitochondria had an enhanced oxidative capacity and sustained fission, which was driven by DRP1.

2. Materials and Methods

2.1. Reagents

Culture media and buffer solutions were purchased from Lonza Verviers (Verviers, Belgium), fetal bovine serum, insulin and trypsin from Invitrogen (Cergy Pontoise, France), hFGF2 from Peprotech (Neuilly sur Seine, France). Other reagents were from Sigma-Aldrich Chimie (Saint-Quentin Fallavier, France).

2.2. hMADS cell culture

The establishment and characterization of hMADS cells has been described [36-39]. Cells were used between passages 14 and 25, all experiments were performed at least 3 times and cells were free of viruses and mycoplasma. Cells were cultured in Dulbecco's modified Eagle's medium (DMEM) supplemented with 10% FBS, 15 mM Hepes and 2.5 ng/ml hFGF2. Cells were triggered for differentiation on the second day post-confluence (designated as day 0) in DMEM/Ham's F12 media supplemented with 10 µg/ml transferrin, 10 nM insulin, 0.2 nM triiodothyronine, 1 µM dexamethasone and 500 µM isobutyl-methylxanthine. Two days later, the medium was changed (dexamethasone and isobutyl-methylxanthine removed) and 100 nM rosiglitazone were added. At day 9, rosiglitazone was withdrawn to enable white adipocyte differentiation. Rosiglitazone (100 nM) or GW7647 (300 nM) were added at day 14 to promote white to brite adipocyte conversion and cells were used at day 18.

Transfection experiments were performed using HiPerfect (QIAGEN, France) at day 14 of differentiation. Cells were incubated with a mixture containing HiPerfect and siRNA (50 nM) in DMEM. Four hours later, it was supplemented with F12 medium containing 20 µg/ml transferrin, 20 nM insulin, and 0.4 nM triiodothyronine. siRNA against human DRP1 is from Ambion (Life Technologies, Courtaboeuf, France) and validated to specifically target DRP1 (ID #: s19560).

2.3. Western blot analysis

Proteins were extracted and blotted as previously described [40]. Primary antibody incubation was performed overnight at 4°C (anti-UCP1, Calbiochem, #662045, dilution 1:750; and anti-β-tubulin, Sigma #T5201, dilution 1:2000; anti-DRP1, Cell Signaling #5391, dilution 1:1000; anti-phosphoDRP1(Ser616), Cell Signaling #4494, dilution 1:1000; anti-citrate synthase, Abcam #ab96600, dilution 1:10000) and then detected with HRP-conjugated anti-rabbit or anti-mouse immunoglobulins (Promega, Charbonnières-les-Bains, France). Detection was performed using Chemiluminescent HRP Substrate (Millipore, Molsheim, France). OD band intensities were evaluated using PCBas Software.

For mitochondrial complex quantitation, equal amounts of cell proteins were separated using gradient SDS-PAGE (10-20%) and blotted onto nitrocellulose membranes. Saturated membranes were incubated overnight with a 1:1000 dilution of total OXPHOS human Western blot antibody cocktail (#MS601, Mitosciences) followed by 60 min incubation with HRP-conjugated anti-mouse immunoglobulins. Chemiluminescence obtained after addition of Clarity ECL Western blotting substrate (BioRad, Marnes-la-Coquette, France) was detected using a ChemiDoc MP Imaging System (Bio-Rad) and quantified with Image Lab 5.0 software (Bio-Rad).

2.4. Immunostaining analysis

Cells were fixed with PAF 4% for 10 min, permeabilized with 0.1% Triton X-100 for 10 min, and then sequentially incubated with primary antibody overnight at 4°C (anti-UCP1, Calbiochem, #662045, dilution 1:100; anti-TIMM23, BD Biosciences #611222, dilution 1:500; anti-cytochrome C, SantaCruzBT #sc-13560, dilution 1:100) and with the relevant secondary antibody coupled to Alexa-488 or Alexa-594 (Invitrogen, dilution 1:500) for 30min at RT. Cells were finally mounted and visualized with an Axiovert microscope (Carl Zeiss, Le Pecq, France) under oil immersion and pictures were captured and treated with AxioVision software (Carl Zeiss). The mitochondrial network was analyzed using Fiji software [41].

2.5. Isolation and analysis of RNA

These procedures were carried out according to MIQE recommendations [42]. Total RNA was extracted using TRI-Reagent (Euromedex, Souffelweyersheim, France) according to the manufacturer's instructions. Reverse transcription-quantitative polymerase chain reaction (RT-qPCR) was conducted as described previously [43]. The expression of selected genes was normalized to that of TATA-box binding protein (TBP) and 36B4 housekeeping genes and then quantified using the comparative-ΔCt method. Primer sequences are available upon request.

2.6. Mitochondrial DNA quantification

DNA was extracted using a DNA extraction kit (Macherey-Nagel EURL, France). 2 ng of the total DNA were used for qPCR analysis, and the mitochondrial DNA content was calculated from the ratio of the DNA of the NADH dehydrogenase subunit 1 gene (mitochondrial gene) to that of lipoprotein lipase gene (a nuclear gene) as previously described [44].

2.7. Oxygen consumption analysis

For respiration analysis, hMADS cells were seeded in a 24 multi-well plate (Seahorse) and differentiated as described previously [45]. The oxygen consumption rate (OCR) of 18-day-old differentiated cells was determined using an XF24 Extracellular Flux Analyzer (Seahorse Bioscience). Uncoupled and maximal OCR were determined using oligomycin (1.2 μM) and FCCP (1 μM). Rotenone and Antimycin-A (2 μM each) were used to inhibit mitochondrial respiration. All parameters were calculated as described previously [46].

2.8. Electron microscopy

hMADS adipocytes were fixed in 1.6% glutaraldehyde in 0.1 M phosphate buffer. They were rinsed with cacodylate buffer, then post-fixed in osmium tetroxide (1%) and reduced with potassium ferrycyanide for 1 h. After a water wash, cells were dehydrated with several incubations in increasing concentrations of ethanol and embedded in Epon resin. Eighty nanometer sections were contrasted with uranyl acetate and lead citrate and then observed with an electron microscope (JEOL JEM 1400) operating at 100 kV. Electron microscopy pictures

displaying omental adipose tissue of patients with pheocromocytoma were described in a previous study [47].

2.9. Statistical analysis

Data were expressed as mean values ± SEM. They were analyzed using InStat3 software (GraphPad Software, CA, USA) by a one-way ANOVA followed by a Student-Newman-Keuls post-test, or a Student's *t*-test to assess any statistical differences between experimental groups. Differences were considered statistically significant when $p < 0.05$.

3. Results

3.1. hMADS brite adipocytes display increased mitochondriogenesis and mitochondrial activity

hMADS cells are able to differentiate into white adipocytes and then convert into functional brite adipocytes when they are treated with rosiglitazone or GW7647, specific agonists of PPARγ and PPARα, respectively [43, 48]. The expression of genes encoding UCP1 (Figure 1a-b) and other classical brown/brite adipocyte markers, such as carnitine-palmitoyltransferase 1B (*CPT1B*) and cell death-inducing DFFA-like effector A (*CIDEA*) (Figure 1c) was significantly higher in hMADS brite adipocytes upon PPARγ or PPARα activation. Likewise, the expression of genes encoding mitochondrial membrane components and respiratory chain subunits displayed similar trends or significant increases the activated hMADS brite adipocytes (Figure 1c). Mitochondrial DNA content, a marker of mitochondriogenesis, was higher in brite compared to white adipocytes (Figure 2a). Levels of the respiratory chain complex proteins were increased (Figure 2b, Supplementary Figure 1a). Specifically, complex II, III and V protein contents were higher in brite adipocytes, while no significant difference was found for complexes I and IV (Figure 2b).

These results suggested an increase in mitochondrial activity in hMADS brite adipocytes. Oxygen consumption analysis (Supplementary Figure 1b) demonstrated that hMADS brite adipocytes displayed higher basal and maximal mitochondrial respiration compared to white fat cells (Figure 2c), as expected given the increase in uncoupled respiration typical of UCP1 activity (Figure 2c). This increased uncoupling respiration was mainly due to the higher expression of UCP1 in brite fat cells. Expression of other protonophoric proteins (*i.e. UCP2*, *UCP3*, *SLC25A4, SLC25A5* and *SLC25A6)* was low and/or unchanged in white and brite adipocytes (data not shown and see references [43, 45]).

3.2. hMADS brite adipocytes display UCP1^{+} round-shaped mitochondria

Mitochondria are able to modulate their morphology from a tubular (fused) to a round (fragmented) shape. These morphological adaptations relate to mitochondrial division and, in various situations, correlate with changes in activity or stress. A recent study performed in rodent brown adipocytes showed that the mitochondria acquired a round shape upon UCP1 activation [34]. Thus, the mitochondrial morphology was analyzed by transmission electron microscopy. Undifferentiated hMADS cells contained a majority of long tubular mitochondria, while hMADS white adipocytes displayed a mix of tubular and partially fragmented mitochondria (Figure 3a and 3b). In contrast, brite adipocytes exhibited round-shaped mitochondria, suggesting sustained fission activity (Figure 3c and 3d). Moreover, mitochondria of brite adipocytes displayed laminar cristae (*i.e.* arranged from side to side of the organelle) (Figure 3c and 3d) compared to the white ones, which were shorter and linear (Figure 3a and 3b) [49]. Analysis of each condition showed that 81 ± 11 % and 89 ± 6 % (mean ± sem) of the mitochondria displayed a round-shaped morphology in brite adipocytes treated with rosiglitazone and GW7647, respectively. In contrast, only 22 ± 6 % exhibited this morphology in white adipocytes. This mitochondrial morphology looked like the one described *in vivo* in murine activated brown adipocytes [34]. To determine the relevance of these results *in vivo* in humans, we analyzed omental WAT of patients with pheocromocytoma by transmission electron microscopy [47]. In these patients, WAT surrounding the tumor displayed activated brite adipocytes due to the high catecholamine secretion by the tumorigenic adrenal gland [47]. Interestingly, mitochondria of these adipocytes displayed the same fragmented morphology and laminar cristae found in hMADS brite adipocytes, which highlights the relevance of this *in vitro* model (Figure 3e).

We performed immunostaining experiments in hMADS adipocytes, to assess the co-localization of UCP1 and TIMM23 (an inner mitochondrial membrane protein used as a mitochondrial marker). Interestingly, UCP1-positive mitochondria displayed a fragmented state while tubular structures were observed in UCP1-negative mitochondria (Figure 4a). These observations were confirmed using another mitochondrial marker, cytochrome c (Figure 4b). Analysis of the

mitochondrial morphology in UCP1-positive and UCP1-negative cells showed that up to 90% of UCP1-positive adipocytes only contained mitochondria with a round-shaped morphology, while the remaining were of both phenotype (Figure 4d and Supplementary Figure 2). In contrast, 60% of the mitochondria in UCP1-negative adipocytes adopted a tubular network, and less than 5% displayed a fragmented phenotype (Figure 4d and Supplementary Figure 2).

3.3. hMADS brite adipocytes display increased DRP1 activation

To determine the mechanisms responsible for fragmentation of brite/beige adipocyte mitochondria, we first analyzed the expression levels of genes involved in mitochondrial fission and fusion. mRNA expression analysis using datasets from omics analyses, available from the Gene Expression Omnibus (GEO) [50] under accession numbers GSE71293 [48] and GSE59703 [45], demonstrated no significant induction of fission gene expression, such as *DNM1L* (also named *DRP1*) or *FIS1*, nor were fusion and mitophagy genes such as *OPA1*, *MFN2*, *PINK* and *PARK2* induced (Supplementary Figure 3a and 3b).

As DRP1 was recently shown to control the fission of mitochondria in rodent brown adipocytes [34], we assessed the phosphorylation of DRP1 on serine 616 (known to activate the human protein) in human white and brite adipocytes. Western blotting experiments clearly showed an increase in DRP1 phosphorylation in both rosiglitazone and GW7647-derived brite adipocytes compared to white fat cells (Figure 4d and Supplementary Figure 4).

3.4. DRP1 knock-down impaired mitochondrial uncoupling respiration in brite adipocytes

To investigate the involvement of DRP1 in human brite adipocyte metabolism, we decreased DRP1 expression using a siRNA approach. hMADS cells were transfected at day 14 of differentiation with 50 nM of DRP1-targeted siRNA, or with a relevant siRNA control, and

subsequently either converted into brite adipocytes or not. DRP1 protein levels decreased by 50% (Figure 5a and Supplementary Figure 5a), without affecting cell mitochondriogenesis *per se*, as citrate synthase and chain respiratory complex level were not affected (Figure 5b-c and Supplementary Figure 6). Additionally, DRP1 knock-down did not reduce adipogenesis and white to brite adipocyte conversion, as was demonstrated by the absence of significant changes in *UCP1* mRNA and protein levels (Figure 5c, Supplementary Figure 6) in siDRP1- compared to siCTRL-treated cells. Similarly, *CPT1B* and *perilipin 1 and 5* mRNA levels were not affected (Figure 5c). We then analyzed respiration in DRP1 knock-down cells (Figure 6a). hMADS brite adipocytes transfected with DRP1 siRNA displayed lower basal (Figure 6b) and uncoupled (Figure 6c) respiration compared to cells transfected with control siRNA. However, maximal respiration (Figure 6d) and the spare respiratory capacity (Figure 6e) were not significantly affected. Thus, a decrease in DRP1 expression disrupted mitochondrial UCP1-dependent oxygen consumption.

In brite adipocytes, UCP1 uncoupling activity is dependent on mitochondrial fatty acid transport, as fatty acids are both oxidized as a substrate [51] and required for UCP1 activation [52]. Inhibition of CPT1B activity, the major fatty acid transporter of adipocyte mitochondria, by acute Etomoxir treatment (50 µM, 2 hours), reduced fatty acid oxidation and the UCP1 uncoupling activity in hMADS brite adipocytes (Figure 7a and [48, 53]). CPT1B inhibition did not affect expression of mitochondrial proteins such as citrate synthase, UCP1 and respiratory chain complex proteins (Figure 7b and Supplementary Figure 6a and 6b). Interestingly, the treatment of brite adipocytes with Etomoxir decreased DRP1 phosphorylation (Figure 7c and Supplementary Figure 6c). These results highlight the relationship between the DRP1 and UCP1 activities in hMADS brite adipocytes.

4. Discussion

Brown and brite adipocytes have drawn considerable attention because of their role in the control of energy balance and metabolism in humans. *In vivo* and *in vitro* studies in rodents have shed light on the mechanisms involved in differentiation, function and activation of these thermogenic-competent adipocytes. In this work, we have characterized the mitochondrial phenotype of human brite adipocytes using hMADS cells, which recapitulate as an *in vitro* model for the conversion of white into brite adipocytes [36, 43, 48, 54], which has been described *in vivo* in mouse white fat depots [23, 55].

The shift from a white- to brite-adipocyte phenotype involves profound changes in the mitochondrial metabolic state [28]. Expression and activation of UCP1 were followed by the increase of oxygen consumption, which was required to maintain ATP synthesis while uncoupling. In addition to higher uncoupling, this increased oxidative capacity in brite adipocytes relied upon active mitochondriogenesis (characterized by a higher mitochondrial DNA content), enhanced respiratory chain activity (characterized by increased maximal respiration and protein levels) and a modification in substrate preference towards fatty acids (increased levels of CPT1B, increased complex II respiratory component and fatty acid oxidation) [48]. Interestingly, the phenotypic modifications in brite adipocytes not only compensated for a decrease in ATP synthesis due to UCP1 uncoupling, but they also endowed brite fat cells with sensitivity to specific stimuli. This latter observation was clearly characterized by the enhanced spare respiratory capacity in brite adipocytes. This parameter illustrated the capacity for substrate supply and electron transport to respond to an increase in energy demand [46]. White adipocytes displayed a very low spare respiratory capacity and thus a poor ability to increase their mitochondrial activity. In contrast, the brite adipocytes were able to sharply increase their oxygen consumption and mitochondrial activity in order to respond to specific stimulation, and thus to increase uncoupling and perform thermogenesis as expected.

In addition to the increased mitochondrial content, previous studies have documented an association between mitochondrial fragmentation and energy expenditure [30, 32], which has been confirmed recently in mouse-derived brown adipocytes [34]. In these cells, mitochondrial fragmentation enhanced mitochondrial uncoupling and energy expenditure and was triggered by the DRP1 activity through its phosphorylation at Ser600. Herein, we demonstrated that mitochondrial fragmentation was associated with UCP1 expression in human adipocytes, as UCP1-positive mitochondria preferentially displayed a round shape, while UCP1-negative mitochondria formed tubular elongated structures. At this stage, hMADS cells treated by PPAR agonists expressed UCP1 and displayed an active brite phenotype, characterized by an increase in uncoupled respiration and oxidative phenotype [48]. We cannot rule out an effect of PPAR pathway activation on mitochondria fragmentation, due to the simultaneous occurrence of PPAR activation, UCP1 expression and activation in hMADS cells. Nevertheless, fragmented mitochondria were not found in undifferentiated hMADS cells treated by rosiglitazone, excluding an effect of PPAR activation on fission events (data not shown).

The fragmentation of mitochondria was associated with increased phosphorylation of DRP1 at Ser616, the equivalent of murine Ser600, which is known to promote mitochondrial fission by CDK1/cyclin B [56]. Interestingly, in hMADS brite adipocytes and mouse brown adipocytes [34], DRP1 regulates UCP1 activity as a decrease in DRP1 expression specifically disrupted mitochondrial uncoupling and associated basal respiration. Of note, fission did not modulate the total mitochondrial oxidative capacity of the cells, since DRP1 knock-down did not significantly change maximal respiration. Our results focused on Ser616 phosphorylation of DRP1, but we cannot exclude other modifications. Indeed, DRP1 can be modulated by numerous post-translational modifications, such as Ser637 phosphorylation, which inhibits DRP1 activity [57], and N-acetyl-glucosamine glycosylation, which potentiates DRP1 activity by inhibition of Ser637 phosphorylation [58].

Our work is consistent with findings in mice, and confirms that mitochondrial fission in human adipocytes may be considered as a physiological adaptation, instead of a purely deleterious mechanism. In rodents, an increase of DRP1 phosphorylation was found in activated BAT and the blocking of mitochondrial fission mildly reduced uncoupled respiration [34]. Herein, we have shown in human brite fat cells that DRP1 phosphorylation correlated with UCP1 expression and that DRP1 knock-down abrogated the increase of uncoupled respiration, which returned to the level found in white adipocytes. DRP1 regulated the activity of brite and brown adipocytes, but did not appear to control the acquisition of the thermogenic phenotype. Indeed, in rodents, it has been demonstrated that mitochondrial fragmentation was only observed after catecholamine stimulation [34]. Similarly, we have shown that DRP1 knock-down did not modify UCP1 expression but only uncoupled respiration. Thus, the link between UCP1 activity and DRP1 activation is yet to be characterized.

As mitochondria morphology is controlled by cycles of fission and fusion events [33], and a fragmented morphology might be due to decreased fusion events in addition to increased fission. In contrast to results reported in rodents [34], our data are not in favor of inhibition of fusion events in this process, as several key components associated with fusion did not display any variation at either RNA or protein levels (data not shown). Nevertheless, further studies are required to characterize the mitochondrial fusion mechanism more precisely in hMADS adipocytes.

We also showed that mitochondrial fragmentation was accompanied by morphological changes in cristae during white to brite adipocyte conversion. Indeed, cristae within white adipocyte mitochondria tended to be linear and short while the cristae of brite adipocyte mitochondria displayed a longer, laminar and curved shape. Given the link between cristae structure and ATP synthase dimerization, these changes in the curvature of the cristae could be related to reduced coupled respiration in favor of uncoupled respiration [34, 59].

5. Conclusion

In conclusion, our data demonstrated that profound mitochondrial modifications occurred during human white to brite adipocyte conversion, and that the mitochondrial fission process described in mouse brown adipocytes also occurs in humans.

ACKNOWLEDGEMENTS. This work was supported by CNRS. The authors acknowledge the CCMA (Centre Commun de Microscopie Appliquée, Université de Nice Sophia Antipolis, Microscopy and Imaging platform Côte d'Azur, MICA) and the Cytomed Platform from IRCAN. DL is a member of Institut Universitaire de France. We thank Dr. Abby Cuttriss for editing the manuscript (http://univ-cotedazur.fr/services/visibilite-internationnale/en).

CONFLICT OF INTEREST. The authors declare no competing financial interests in relation to the work described.

AUTHOR CONTRIBUTION. Conceived and designed the experiments: DFP, EZA. Performed the experiments: DFP, VB, JCC, DB, RAG, MG, AM, SP, SC. Analyzed the data: DFP, VB, SC, DL, EZA. Wrote the manuscript: DFP, VB, DL, EZA.

REFERENCES.

[1] Kopecky J., Clarke G., Enerback S., Spiegelman B., Kozak L.P., 1995. Expression of the mitochondrial uncoupling protein gene from the aP2 gene promoter prevents genetic obesity. J. Clin. Invest. 96:2914-2923.
[2] Langin D., 2010. Recruitment of brown fat and conversion of white into brown adipocytes: strategies to fight the metabolic complications of obesity? Biochim. Biophys. Acta 1801:372-376.
[3] Cannon B., Nedergaard J., 2004. Brown adipose tissue: function and physiological significance. Physiol. Rev. 84:277-359.
[4] Chondronikola M., Volpi E., Borsheim E., Porter C., Annamalai P., Enerback S., Lidell M.E., Saraf M.K., Labbe S.M., Hurren N.M., Yfanti C., Chao T., Andersen C.R., Cesani F., Hawkins H., Sidossis L.S., 2014. Brown Adipose Tissue Improves Whole Body Glucose Homeostasis and Insulin Sensitivity in Humans. Diabetes.
[5] Feldmann H.M., Golozoubova V., Cannon B., Nedergaard J., 2009. UCP1 ablation induces obesity and abolishes diet-induced thermogenesis in mice exempt from thermal stress by living at thermoneutrality. Cell metabolism 9:203-209.
[6] Ouellet V., Labbe S.M., Blondin D.P., Phoenix S., Guerin B., Haman F., Turcotte E.E., Richard D., Carpentier A.C., 2012. Brown adipose tissue oxidative metabolism contributes to energy expenditure during acute cold exposure in humans. J. Clin. Invest. 122:545-552.
[7] Yoneshiro T., Aita S., Matsushita M., Kayahara T., Kameya T., Kawai Y., Iwanaga T., Saito M., 2013. Recruited brown adipose tissue as an antiobesity agent in humans. J. Clin. Invest. 123:3404-3408.
[8] Enerback S., 2010. Human brown adipose tissue. Cell metabolism 11:248-252.
[9] Harms M., Seale P., 2013. Brown and beige fat: development, function and therapeutic potential. Nat. Med. 19:1252-1263.
[10] Cypess A.M., Lehman S., Williams G., Tal I., Rodman D., Goldfine A.B., Kuo F.C., Palmer E.L., Tseng Y.H., Doria A., Kolodny G.M., Kahn C.R., 2009. Identification and importance of brown adipose tissue in adult humans. N. Engl. J. Med. 360:1509-1517.
[11] Cypess A.M., White A.P., Vernochet C., Schulz T.J., Xue R., Sass C.A., Huang T.L., Roberts-Toler C., Weiner L.S., Sze C., Chacko A.T., Deschamps L.N., Herder L.M., Truchan N., Glasgow A.L., Holman A.R., Gavrila A., Hasselgren P.O., Mori M.A., Molla M., Tseng Y.H., 2013. Anatomical localization, gene expression profiling and functional characterization of adult human neck brown fat. Nat. Med. 19:635-639.
[12] Jespersen N.Z., Larsen T.J., Peijs L., Daugaard S., Homoe P., Loft A., de Jong J., Mathur N., Cannon B., Nedergaard J., Pedersen B.K., Moller K., Scheele C., 2013. A classical brown adipose tissue mRNA signature partly overlaps with brite in the supraclavicular region of adult humans. Cell metabolism 17:798-805.
[13] Sharp L.Z., Shinoda K., Ohno H., Scheel D.W., Tomoda E., Ruiz L., Hu H., Wang L., Pavlova Z., Gilsanz V., Kajimura S., 2012. Human BAT possesses molecular signatures that resemble beige/brite cells. PLoS One 7:e49452.
[14] van Marken Lichtenbelt W.D., Vanhommerig J.W., Smulders N.M., Drossaerts J.M., Kemerink G.J., Bouvy N.D., Schrauwen P., Teule G.J., 2009. Cold-activated brown adipose tissue in healthy men. N. Engl. J. Med. 360:1500-1508.
[15] Virtanen K.A., Lidell M.E., Orava J., Heglind M., Westergren R., Niemi T., Taittonen M., Laine J., Savisto N.J., Enerback S., Nuutila P., 2009. Functional brown adipose tissue in healthy adults. N. Engl. J. Med. 360:1518-1525.
[16] Wu J., Bostrom P., Sparks L.M., Ye L., Choi J.H., Giang A.H., Khandekar M., Virtanen K.A., Nuutila P., Schaart G., Huang K., Tu H., van Marken Lichtenbelt W.D., Hoeks J., Enerback S., Schrauwen P.,

Spiegelman B.M., 2012. Beige adipocytes are a distinct type of thermogenic fat cell in mouse and human. Cell 150:366-376.
[17] Zingaretti M.C., Crosta F., Vitali A., Guerrieri M., Frontini A., Cannon B., Nedergaard J., Cinti S., 2009. The presence of UCP1 demonstrates that metabolically active adipose tissue in the neck of adult humans truly represents brown adipose tissue. FASEB J. 23:3113-3120.
[18] Cederberg A., Gronning L.M., Ahren B., Tasken K., Carlsson P., Enerback S., 2001. FOXC2 is a winged helix gene that counteracts obesity, hypertriglyceridemia, and diet-induced insulin resistance. Cell 106:563-573.
[19] Cohen P., Levy J.D., Zhang Y., Frontini A., Kolodin D.P., Svensson K.J., Lo J.C., Zeng X., Ye L., Khandekar M.J., Wu J., Gunawardana S.C., Banks A.S., Camporez J.P., Jurczak M.J., Kajimura S., Piston D.W., Mathis D., Cinti S., Shulman G.I., Seale P., Spiegelman B.M., 2014. Ablation of PRDM16 and Beige Adipose Causes Metabolic Dysfunction and a Subcutaneous to Visceral Fat Switch. Cell 156:304-316.
[20] Leonardsson G., Steel J.H., Christian M., Pocock V., Milligan S., Bell J., So P.W., Medina-Gomez G., Vidal-Puig A., White R., Parker M.G., 2004. Nuclear receptor corepressor RIP140 regulates fat accumulation. Proc. Natl. Acad. Sci. U. S. A. 101:8437-8442.
[21] Seale P., Conroe H.M., Estall J., Kajimura S., Frontini A., Ishibashi J., Cohen P., Cinti S., Spiegelman B.M., 2011. Prdm16 determines the thermogenic program of subcutaneous white adipose tissue in mice. J. Clin. Invest. 121:96-105.
[22] Lee Y.H., Petkova A.P., Konkar A.A., Granneman J.G., 2015. Cellular origins of cold-induced brown adipocytes in adult mice. FASEB J. 29:286-299.
[23] Rosenwald M., Perdikari A., Rulicke T., Wolfrum C., 2013. Bi-directional interconversion of brite and white adipocytes. Nat. Cell Biol. 15:659-667.
[24] Wang Q.A., Tao C., Gupta R.K., Scherer P.E., 2013. Tracking adipogenesis during white adipose tissue development, expansion and regeneration. Nat. Med. 19:1338-1344.
[25] Cinti S., 2009. Transdifferentiation properties of adipocytes in the adipose organ. Am. J. Physiol. Endocrinol. Metab. 297:E977-986.
[26] Lee Y.H., Mottillo E.P., Granneman J.G., 2014. Adipose tissue plasticity from WAT to BAT and in between. Biochim. Biophys. Acta 1842:358-369.
[27] Nedergaard J., Golozoubova V., Matthias A., Asadi A., Jacobsson A., Cannon B., 2001. UCP1: the only protein able to mediate adaptive non-shivering thermogenesis and metabolic inefficiency. Biochim. Biophys. Acta 1504:82-106.
[28] Shabalina I.G., Petrovic N., de Jong J.M., Kalinovich A.V., Cannon B., Nedergaard J., 2013. UCP1 in brite/beige adipose tissue mitochondria is functionally thermogenic. Cell reports 5:1196-1203.
[29] Vernochet C., Mourier A., Bezy O., Macotela Y., Boucher J., Rardin M.J., An D., Lee K.Y., Ilkayeva O.R., Zingaretti C.M., Emanuelli B., Smyth G., Cinti S., Newgard C.B., Gibson B.W., Larsson N.G., Kahn C.R., 2012. Adipose-specific deletion of TFAM increases mitochondrial oxidation and protects mice against obesity and insulin resistance. Cell metabolism 16:765-776.
[30] Liesa M., Shirihai O.S., 2013. Mitochondrial dynamics in the regulation of nutrient utilization and energy expenditure. Cell metabolism 17:491-506.
[31] Gomes L.C., Di Benedetto G., Scorrano L., 2011. During autophagy mitochondria elongate, are spared from degradation and sustain cell viability. Nat. Cell Biol. 13:589-598.
[32] Molina A.J., Wikstrom J.D., Stiles L., Las G., Mohamed H., Elorza A., Walzer G., Twig G., Katz S., Corkey B.E., Shirihai O.S., 2009. Mitochondrial networking protects beta-cells from nutrient-induced apoptosis. Diabetes 58:2303-2315.
[33] Twig G., Shirihai O.S., 2011. The interplay between mitochondrial dynamics and mitophagy. Antioxid Redox Signal 14:1939-1951.
[34] Wikstrom J.D., Mahdaviani K., Liesa M., Sereda S.B., Si Y., Las G., Twig G., Petrovic N., Zingaretti C., Graham A., Cinti S., Corkey B.E., Cannon B., Nedergaard J., Shirihai O.S., 2014. Hormone-induced

mitochondrial fission is utilized by brown adipocytes as an amplification pathway for energy expenditure. EMBO J. 33:418-436.
[35] Beranger G.E., Karbiener M., Barquissau V., Pisani D.F., Scheideler M., Langin D., Amri E.Z., 2013. In vitro brown and "brite"/"beige" adipogenesis: human cellular models and molecular aspects. Biochim. Biophys. Acta 1831:905-914.
[36] Elabd C., Chiellini C., Carmona M., Galitzky J., Cochet O., Petersen R., Penicaud L., Kristiansen K., Bouloumie A., Casteilla L., Dani C., Ailhaud G., Amri E.Z., 2009. Human multipotent adipose-derived stem cells differentiate into functional brown adipocytes. Stem Cells 27:2753-2760.
[37] Rodriguez A.M., Elabd C., Delteil F., Astier J., Vernochet C., Saint-Marc P., Guesnet J., Guezennec A., Amri E.Z., Dani C., Ailhaud G., 2004. Adipocyte differentiation of multipotent cells established from human adipose tissue. Biochem. Biophys. Res. Commun. 315:255-263.
[38] Rodriguez A.M., Pisani D., Dechesne C.A., Turc-Carel C., Kurzenne J.Y., Wdziekonski B., Villageois A., Bagnis C., Breittmayer J.P., Groux H., Ailhaud G., Dani C., 2005. Transplantation of a multipotent cell population from human adipose tissue induces dystrophin expression in the immunocompetent mdx mouse. J. Exp. Med. 201:1397-1405.
[39] Zaragosi L.E., Ailhaud G., Dani C., 2006. Autocrine fibroblast growth factor 2 signaling is critical for self-renewal of human multipotent adipose-derived stem cells. Stem Cells 24:2412-2419.
[40] Pisani D.F., Ghandour R.A., Beranger G.E., Le Faouder P., Chambard J.C., Giroud M., Vegiopoulos A., Djedaini M., Bertrand-Michel J., Tauc M., Herzig S., Langin D., Ailhaud G., Duranton C., Amri E.Z., 2014. The omega6-fatty acid, arachidonic acid, regulates the conversion of white to brite adipocyte through a prostaglandin/calcium mediated pathway. Molecular metabolism 3:834-847.
[41] Schindelin J., Arganda-Carreras I., Frise E., Kaynig V., Longair M., Pietzsch T., Preibisch S., Rueden C., Saalfeld S., Schmid B., Tinevez J.Y., White D.J., Hartenstein V., Eliceiri K., Tomancak P., Cardona A., 2012. Fiji: an open-source platform for biological-image analysis. Nat Methods 9:676-682.
[42] Bustin S.A., Benes V., Garson J.A., Hellemans J., Huggett J., Kubista M., Mueller R., Nolan T., Pfaffl M.W., Shipley G.L., Vandesompele J., Wittwer C.T., 2009. The MIQE guidelines: minimum information for publication of quantitative real-time PCR experiments. Clin. Chem. 55:611-622.
[43] Pisani D.F., Djedaini M., Beranger G.E., Elabd C., Scheideler M., Ailhaud G., Amri E.Z., 2011. Differentiation of Human Adipose-Derived Stem Cells into "Brite" (Brown-in-White) Adipocytes. Front. Endocrinol. (Lausanne) 2:87.
[44] Bordicchia M., Liu D., Amri E.Z., Ailhaud G., Dessi-Fulgheri P., Zhang C., Takahashi N., Sarzani R., Collins S., 2012. Cardiac natriuretic peptides act via p38 MAPK to induce the brown fat thermogenic program in mouse and human adipocytes. J. Clin. Invest. 122:1022-1036.
[45] Loft A., Forss I., Siersbaek M.S., Schmidt S.F., Larsen A.S., Madsen J.G., Pisani D.F., Nielsen R., Aagaard M.M., Mathison A., Neville M.J., Urrutia R., Karpe F., Amri E.Z., Mandrup S., 2015. Browning of human adipocytes requires KLF11 and reprogramming of PPARgamma superenhancers. Genes Dev. 29:7-22.
[46] Brand M.D., Nicholls D.G., 2011. Assessing mitochondrial dysfunction in cells. Biochem. J. 435:297-312.
[47] Frontini A., Vitali A., Perugini J., Murano I., Romiti C., Ricquier D., Guerrieri M., Cinti S., 2013. White-to-brown transdifferentiation of omental adipocytes in patients affected by pheochromocytoma. Biochim. Biophys. Acta 1831:950-959.
[48] Barquissau V., Beuzelin D., Pisani D.F., Beranger G.E., Mairal A., Montagner A., Roussel B., Tavernier G., Marques M.A., Moro C., Guillou H., Amri E.Z., Langin D., 2016. White-to-brite conversion in human adipocytes promotes metabolic reprogramming towards fatty acid anabolic and catabolic pathways. Molecular metabolism 5:352-365.
[49] Frontini A., Cinti S., 2010. Distribution and development of brown adipocytes in the murine and human adipose organ. Cell metabolism 11:253-256.

[50] Edgar R., Domrachev M., Lash A.E., 2002. Gene Expression Omnibus: NCBI gene expression and hybridization array data repository. Nucleic Acids Res. 30:207-210.
[51] Calderon-Dominguez M., Mir J.F., Fucho R., Weber M., Serra D., Herrero L., 2016. Fatty acid metabolism and the basis of brown adipose tissue function. Adipocyte 5:98-118.
[52] Shabalina I.G., Backlund E.C., Bar-Tana J., Cannon B., Nedergaard J., 2008. Within brown-fat cells, UCP1-mediated fatty acid-induced uncoupling is independent of fatty acid metabolism. Biochim. Biophys. Acta 1777:642-650.
[53] Calderon-Dominguez M., Sebastian D., Fucho R., Weber M., Mir J.F., Garcia-Casarrubios E., Obregon M.J., Zorzano A., Valverde A.M., Serra D., Herrero L., 2016. Carnitine Palmitoyltransferase 1 Increases Lipolysis, UCP1 Protein Expression and Mitochondrial Activity in Brown Adipocytes. PLoS One 11:e0159399.
[54] Ghandour R.A., Giroud M., Vegiopoulos A., Herzig S., Ailhaud G., Amri E.Z., Pisani D.F., 2016. IP-receptor and PPARs trigger the conversion of human white to brite adipocyte induced by carbaprostacyclin. Biochim. Biophys. Acta 1861:285-293.
[55] Barbatelli G., Murano I., Madsen L., Hao Q., Jimenez M., Kristiansen K., Giacobino J.P., De Matteis R., Cinti S., 2010. The emergence of cold-induced brown adipocytes in mouse white fat depots is determined predominantly by white to brown adipocyte transdifferentiation. Am. J. Physiol. Endocrinol. Metab. 298:E1244-1253.
[56] Knott A.B., Bossy-Wetzel E., 2008. Impairing the mitochondrial fission and fusion balance: a new mechanism of neurodegeneration. Ann. N. Y. Acad. Sci. 1147:283-292.
[57] Chang C.R., Blackstone C., 2007. Cyclic AMP-dependent protein kinase phosphorylation of Drp1 regulates its GTPase activity and mitochondrial morphology. J. Biol. Chem. 282:21583-21587.
[58] Gawlowski T., Suarez J., Scott B., Torres-Gonzalez M., Wang H., Schwappacher R., Han X., Yates J.R., 3rd, Hoshijima M., Dillmann W., 2012. Modulation of dynamin-related protein 1 (DRP1) function by increased O-linked-beta-N-acetylglucosamine modification (O-GlcNAc) in cardiac myocytes. J. Biol. Chem. 287:30024-30034.
[59] Paumard P., Vaillier J., Coulary B., Schaeffer J., Soubannier V., Mueller D.M., Brethes D., di Rago J.P., Velours J., 2002. The ATP synthase is involved in generating mitochondrial cristae morphology. EMBO J. 21:221-230.

Figure legends.

Figure 1. Characterization of white to brite adipocyte conversion. hMADS cells were differentiated into white or brite adipocytes using rosiglitazone (brite-R) or GW7647 (brite-G). Adipocytes were analyzed as follows: (a) *UCP1* mRNA expression evaluated by RT-qPCR. (b) Representative images of UCP1 immunostaining, DAPI was used to counterstain nuclei. Scale bar: 100 µm. (c) Brite adipocyte and mitochondrial marker gene expression was evaluated by RT-qPCR. Histograms display means ± SEM of 6 independent samples. *a* = $p<0.05$ *vs*. white, *b* = $p<0.05$ *vs.* brite-R;

Figure 2. Mitochondrial content and activity of human brite adipocytes. hMADS cells were differentiated into white or brite adipocytes using rosiglitazone (brite-R) or GW7647 (brite-G). (a) Mitochondrial DNA content was evaluated by qPCR. (b) Respiratory chain complex expression was analyzed by Western blotting using a specific antibody for one component of each complex (I to V). Histograms display means ± SEM of 6 independent samples. (c) Mitochondrial oxygen consumption was analyzed in differentiated hMADS cells. Histograms display means ± SEM of 21 independent samples. *a*: $p<0.05$ *vs.* white; *b*: $p<0.05$ *vs.* brite-R.

Figure 3. Electron microscopy of white and brite adipocyte mitochondria. (a) Undifferentiated, (b) white- and (c, d) brite-differentiated (either (c) by rosiglitazone, "brite-R", or (d) by GW7647, "brite-G") hMADS cells as well as (e) omental adipose tissue from a patient with pheochromocytoma were analyzed by electron microscopy. Scale bar = 1 µm. L: lipid droplet. Black arrow heads shown example of laminar cristae.

Figure 4. Characterization of UCP1^{+} mitochondrial morphology. (a) and (b) hMADS cells were differentiated into brite adipocytes and then analyzed by immunostaining using a rabbit polyclonal antibody against UCP1 (red) and a monoclonal mouse antibody targeting the

mitochondria ubiquitous protein TIMM23 (green, panel (a)) or cytochrome C (green, panel (b)). (c) Percentage of UCP1-positive and –negative cells (assessed by UCP1 immunostaining) displaying fragmented or tubular mitochondria, or a mixed phenotype (assessed by TIMM23 immunostaining). Histogram displaying the results of 100 white and brite adipocytes. (d) DRP1 phosphorylation was evaluated by Western blotting (left panel) and quantified as phosphoDRP1-Ser616/total-DRP1 ratio (right panel). Histograms display the means ± SEM of 4 independent samples. *a* = p<0.05 *vs.* white. Uncropped blots are displayed in Supplementary Figure 4.

Figure 5. DRP1 knock-down does not modify brite adipocyte formation. hMADS cells were differentiated into brite adipocytes using rosiglitazone (brite-R) and transfected with anti-DRP1 siRNA or control siRNA (50 nM at day 14). (a) DRP1 expression was evaluated by Western blotting, β-tubulin was used as loading control. Band intensities were quantified and expressed as a ratio between DRP1 and β-tubulin. (b) Western blot analysis of citrate synthase, UCP1 and respiratory chain complex protein levels in control and anti-DRP1 siRNA transfected cells. (c) qPCR analysis of *citrate synthase*, *UCP1*, *CPT1B, perilipin 1*, and *perilipin 5* mRNA levels. Histogram display means ± SEM of 3 (a) or 6 (c) independent samples. *a* = p<0.05 *vs.* white; *b* = p<0.05 *vs.* brite-R. Uncropped blots are displayed in Supplementary Figure 5a and 6.

Figure 6. DRP1 knock-down disrupted oxygen consumption linked to UCP1. hMADS adipocytes were analyzed with a Seahorse XF24 device to evaluate the mitochondrial oxygen consumption after DRP1 knock-down. Histogram displaying means ± SEM of 21 independent samples. *a* = p<0.05 *vs.* white; *b* = p<0.05 *vs.* brite-R.

Figure 7. CPT1B inhibition disrupts UCP1 activity and DRP1 phosphorylation. hMADS cells were differentiated into brite adipocytes using rosiglitazone (brite-R) and treated for the final

4 hours with 50 µM Etomoxir. (a) hMADS adipocytes were analyzed with a Seahorse XF24 device to evaluate the mitochondrial oxygen consumption after Etomoxir treatment. (b) Western blot analysis of citrate synthase, UCP1 and respiratory chain complex protein levels in control and Etomoxir treated cells. (c) DRP1 phosphorylation was evaluated by Western blotting and quantified as the phosphoDRP-Ser616/total DRP1 ratio. Histogram displaying means ± SEM of 14 (a) and 3 (c) independent samples. *a* = $p<0.05$ *vs.* white; *b* = $p<0.05$ *vs.* brite-R. Uncropped blots are displayed in Supplementary Figure 5b and 6.

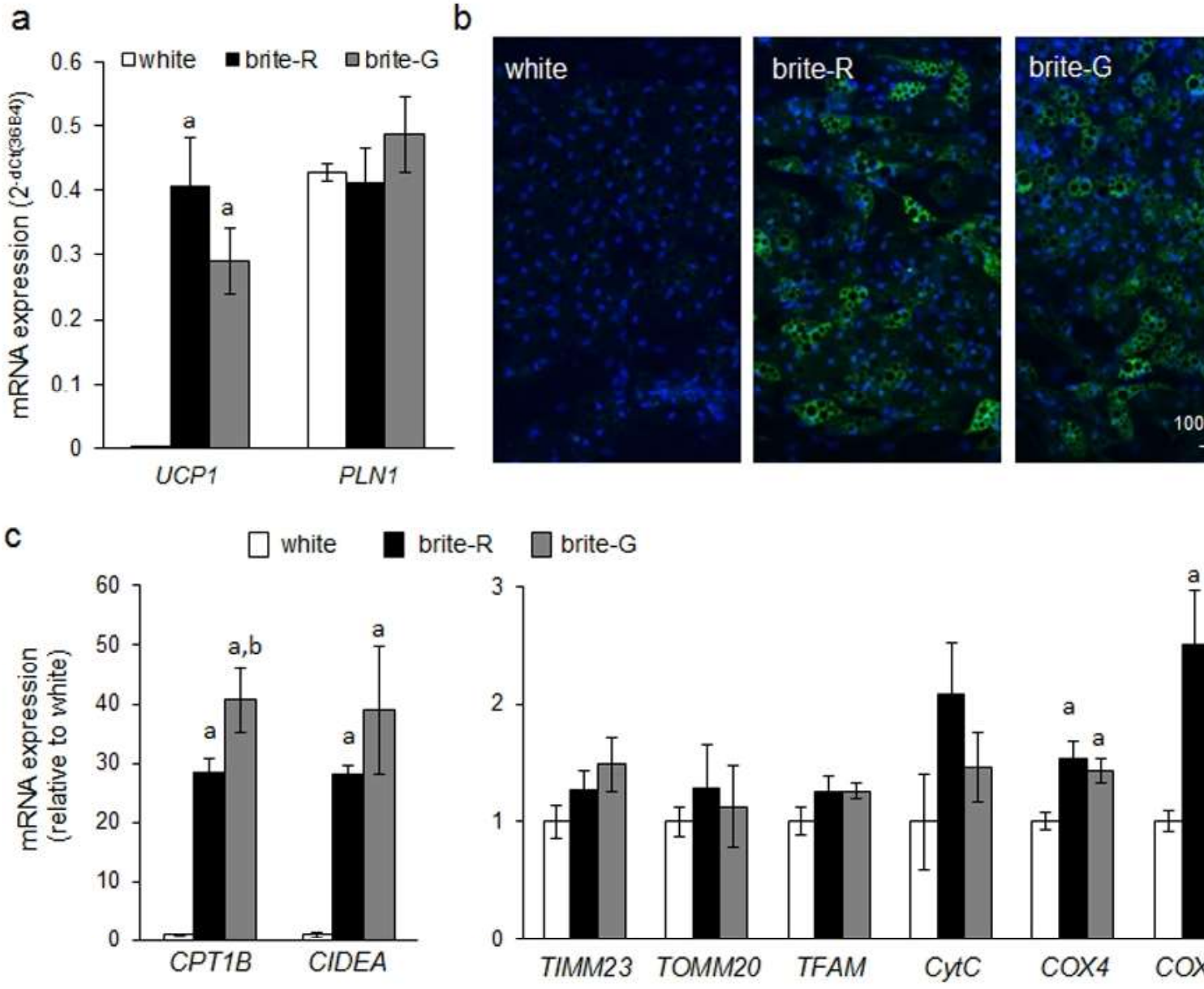
a
white
brite-R
brite-G
mRNA expression (2-dCt(36B4))
0.6
0.5
0.4
0.3
0.2
0.1
0
a
a
UCP1
PLN1
b
white
brite-R
brite-G
100
c
white
brite-R
brite-G
mRNA expression (relative to white)
60
50
40
30
20
10
0
a
a,b
a
a
CPT1B
CIDEA
3
2
1
0
a
a
a
TIMM23
TOMM20
TFAM
CytC
COX4
COX

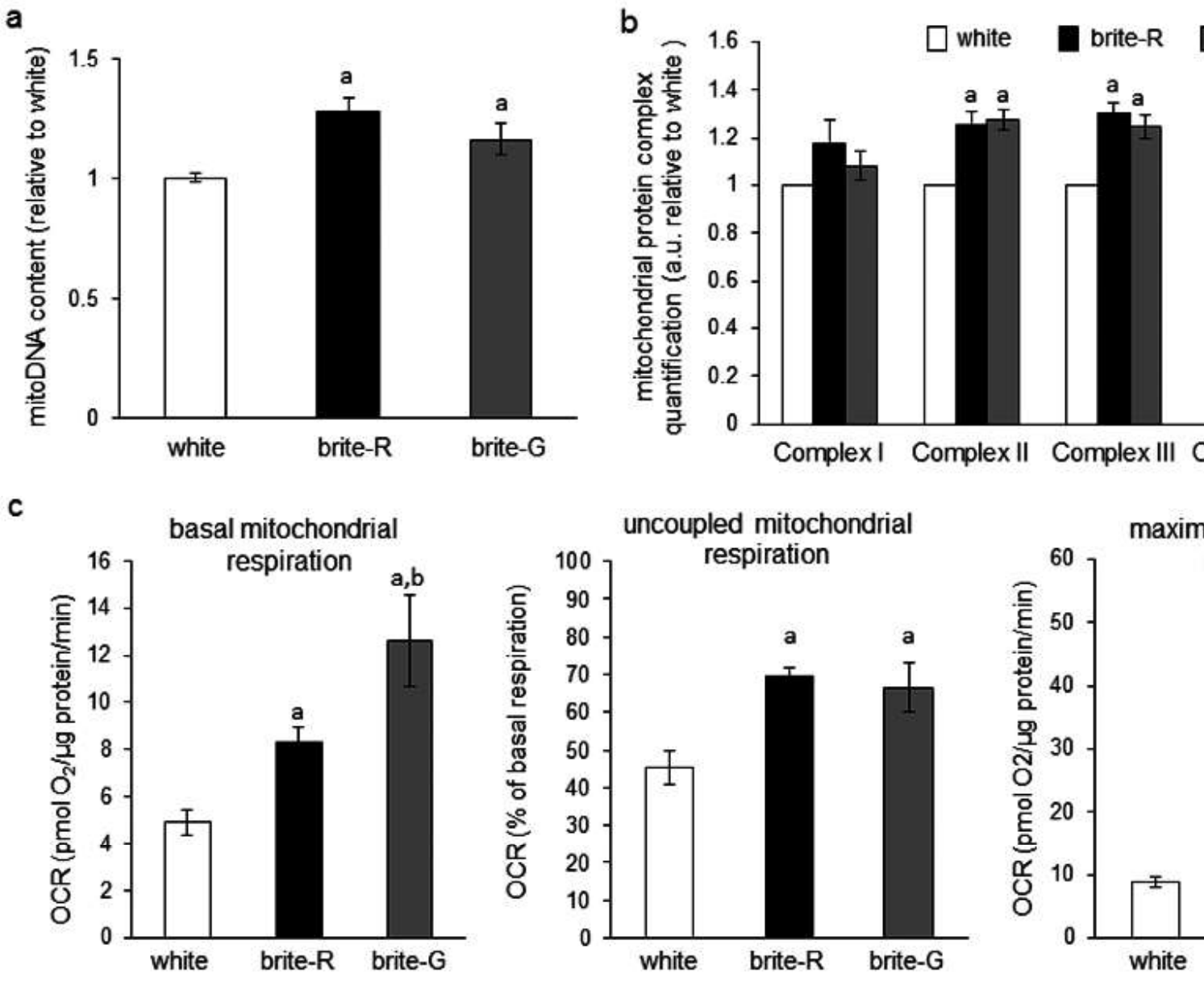
a
mitoDNA content (relative to white)
1.5
1
0.5
0
a
a
white
brite-R
brite-G
b
white
brite-R
mitochondrial protein complex quantification (a.u. relative to white)
1.6
1.4
1.2
1
0.8
0.6
0.4
0.2
0
a
a
a
a
Complex I
Complex II
Complex III
c
basal mitochondrial respiration
OCR (pmol O2/µg protein/min)
16
14
12
10
8
6
4
2
0
a
a,b
white
brite-R
brite-G
uncoupled mitochondrial respiration
OCR (% of basal respiration)
100
90
80
70
60
50
40
30
20
10
0
a
a
white
brite-R
brite-G
maxim
OCR (pmol O2/µg protein/min)
60
50
40
30
20
10
0
white

a
undifferentiated hMADS cells
b
hMADS
adipocytes - white
c
hMADS adipocytes - brite-R
L
d
hMADS adipocytes - brite-G
e
in vivo brite adipocyte– omental fat
from pheochromocytoma patient
L
L
L

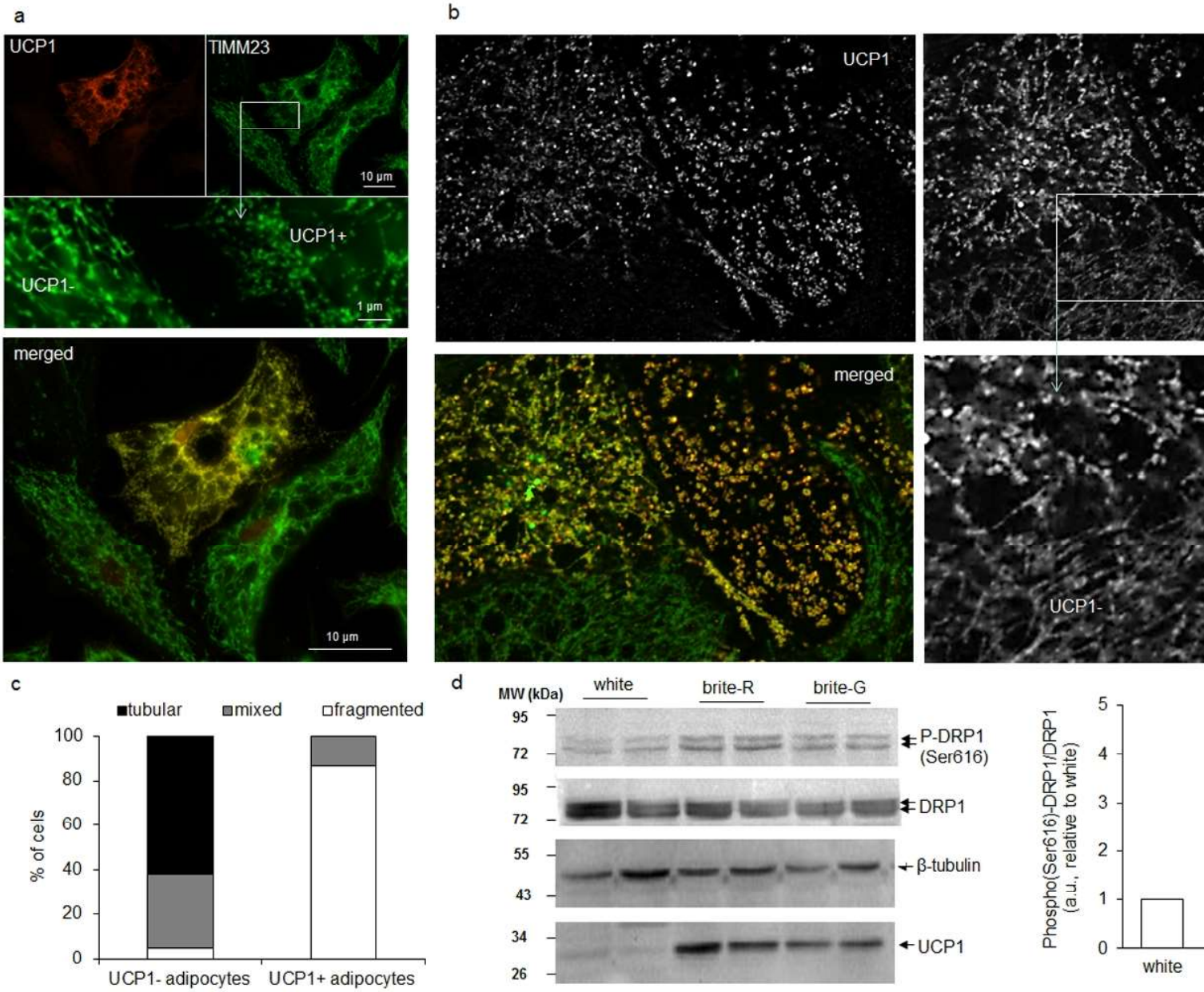
a
UCP1
TIMM23
10 µm
UCP1+
UCP1-
1 µm
merged
10 µm
b
UCP1
merged
UCP1-
c
tubular
mixed
fragmented
100
80
60
40
20
0
% of cells
UCP1- adipocytes
UCP1+ adipocytes
d
MW (kDa)
white
brite-R
brite-G
95
72
P-DRP1
(Ser616)
95
72
DRP1
55
43
β-tubulin
34
26
UCP1
Phospho(Ser616)-DRP1/DRP1
(a.u., relative to white)
5
4
3
2
1
0
white

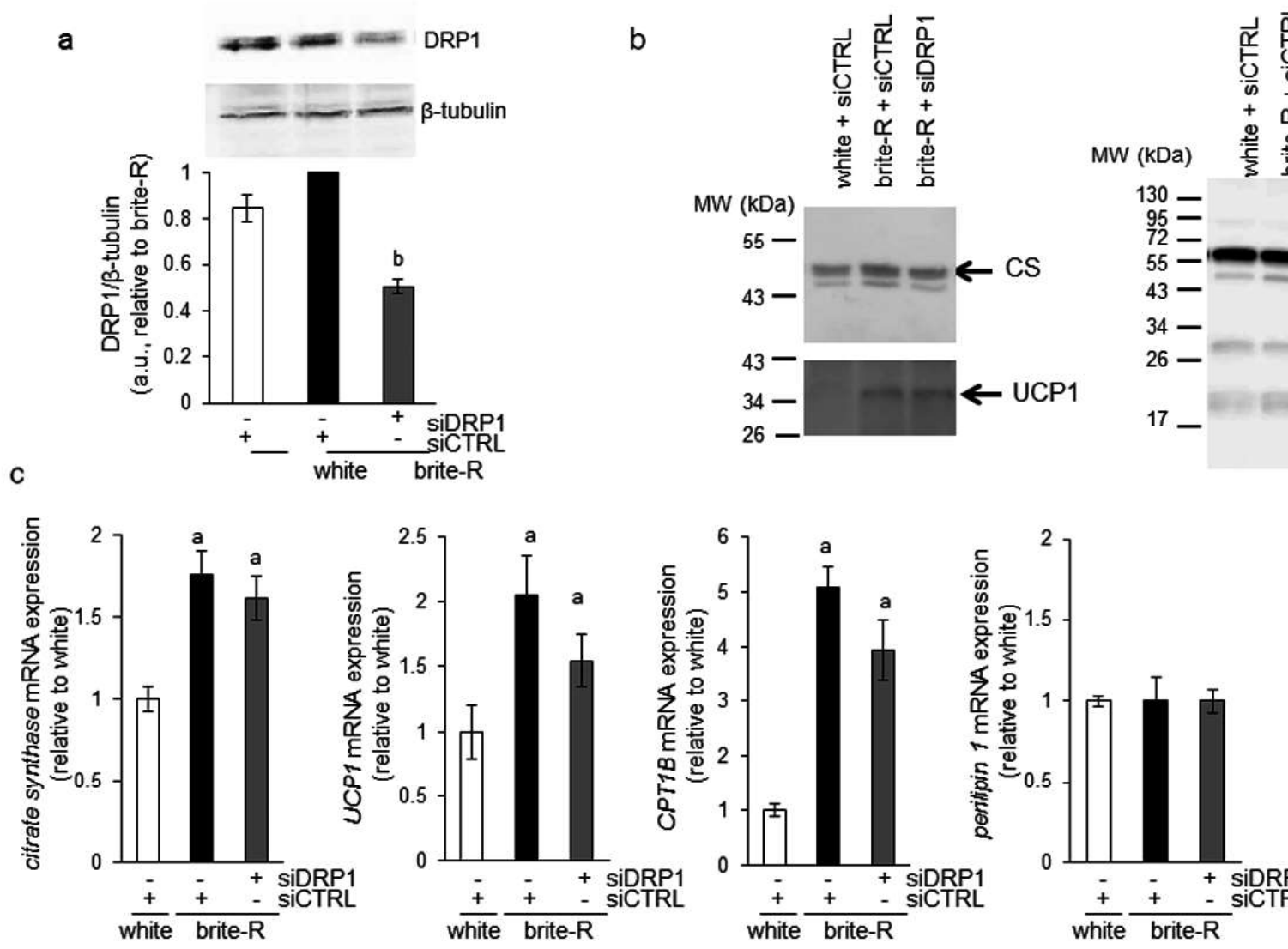
a
DRP1
β-tubulin
DRP1/β-tubulin (a.u., relative to brite-R)
b
siDRP1
siCTRL
white
brite-R
b
white + siCTRL
brite-R + siCTRL
brite-R + siDRP1
MW (kDa)
CS
UCP1
c
citrate synthase mRNA expression (relative to white)
UCP1 mRNA expression (relative to white)
CPT1B mRNA expression (relative to white)
perilipin 1 mRNA expression (relative to white)
a
siDRP1
siCTRL
white
brite-R

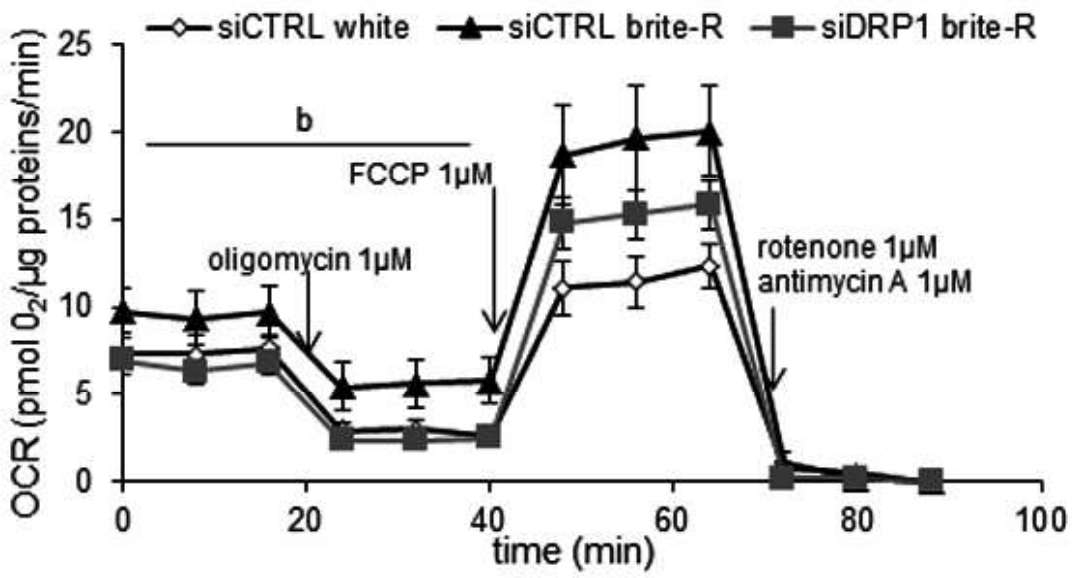
siCTRL white
siCTRL brite-R
siDRP1 brite-R
OCR (pmol O2/µg proteins/min)
b
FCCP 1µM
oligomycin 1µM
rotenone 1µM
antimycin A 1µM
time (min)

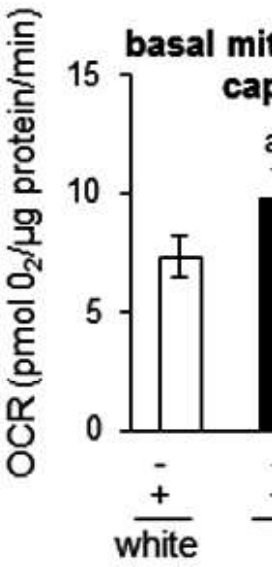
basal mit
cap
OCR (pmol O2/µg protein/min)
white

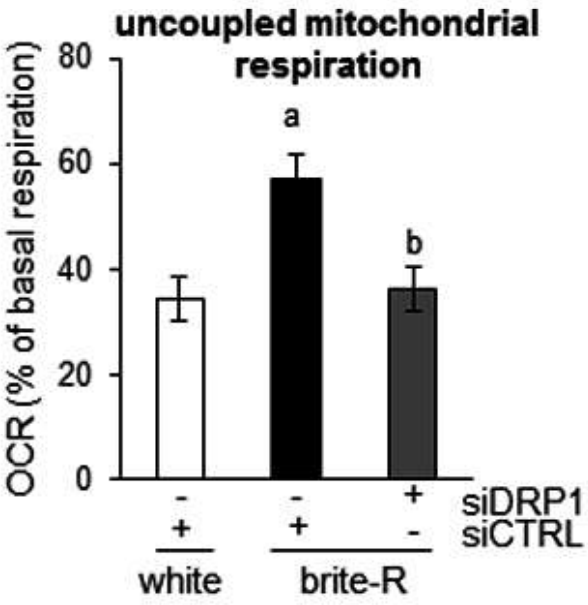
uncoupled mitochondrial respiration
OCR (% of basal respiration)
a
b
siDRP1
siCTRL
white
brite-R

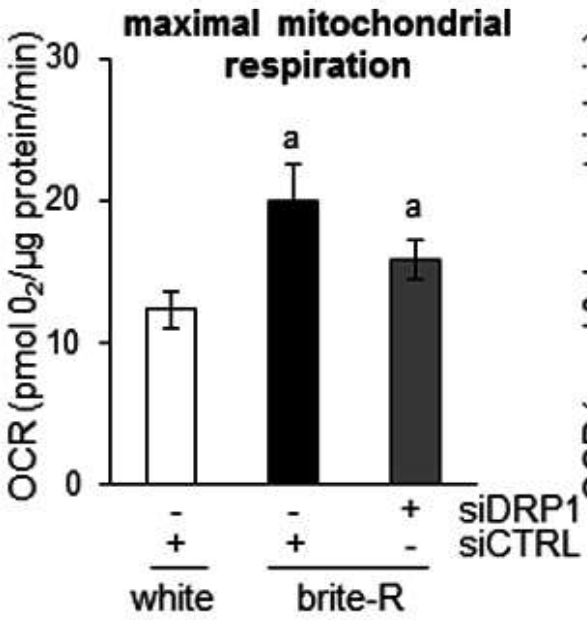
maximal mitochondrial respiration
OCR (pmol O2/µg protein/min)
a
a
siDRP1
siCTRL
white
brite-R

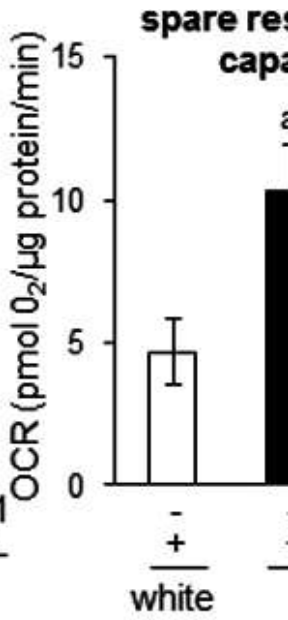
spare res
capa
OCR (pmol O2/µg protein/min)
white

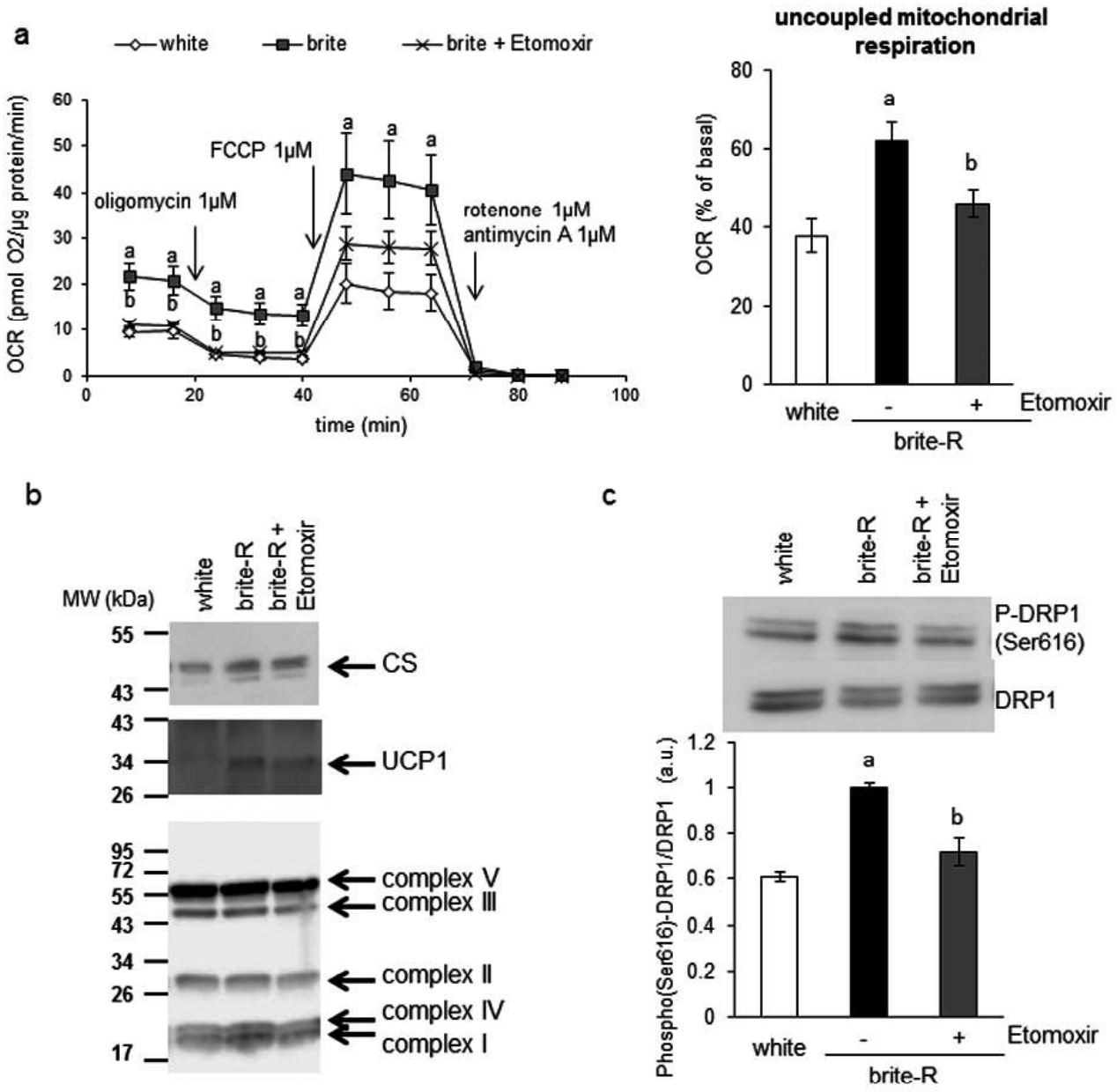
a
white
brite
brite + Etomoxir
OCR (pmol O2/µg protein/min)
time (min)
oligomycin 1µM
FCCP 1µM
rotenone 1µM
antimycin A 1µM
uncoupled mitochondrial respiration
OCR (% of basal)
white
brite-R
Etomoxir
b
MW (kDa)
white
brite-R
brite-R + Etomoxir
CS
UCP1
complex V
complex III
complex II
complex IV
complex I
c
P-DRP1 (Ser616)
DRP1
Phospho(Ser616)-DRP1/DRP1 (a.u.)

CONFLICT OF INTEREST. The authors declare having no conflict of interest.

APPENDIX A. SUPPORTING INFORMATION

Supplementary Figure 1. Respiratory chain complex quantification. (a) hMADS cells were differentiated into white or brite adipocytes using rosiglitazone (brite-R) or GW7647 (brite-G) and harvested for protein extraction. Representative Western blot of mitochondrial complexes (I to V). Quantification of the total amount of respiratory chain complexes. Values represent means ± SEM of at least 3 independent experiments; a = $p<0.05$ vs. white. (b) hMADS cells were differentiated into white or in brite adipocytes using rosiglitazone (brite-R) or GW7647 (brite-G) and then analyzed with a Seahorse XF24 device to evaluate the mitochondrial oxygen consumption. Histograms displaying the spare respiratory capacity (SRC) are mean ± SEM of 21 samples. *a* = $p<0.05$ vs. white; *b* = $p<0.05$ vs. brite-R.

Supplementary Figure 2. Typical images of immunofluorescence used for evaluation of the mitochondria morphology in Figure 4D.

Supplementary Figure 3. Expression of fusion and fission mitochondrial genes. hMADS cells were differentiated into white or brite adipocytes using rosiglitazone (brite-R) or GW7647 (brite-G) and harvested for RNA or protein extraction. Analysis of the expression of various genes of key fusion and fission proteins by (a) microarray (GEO accession number GSE71293) or (b) RNAseq approaches (GEO accession number GSE59703). Histograms display mean ± SEM of 3 experiments; RPKM = Reads Per Kilobase per Million mapped reads.

Supplementary Figure 4. Uncropped and additional Western blots used in Figures 4d.

Supplementay Figure 5. Uncropped and additional Western blots used in Figures 5a.

Supplementay Figure 6. Uncropped and additional Western blot used in Figures 5b, 7b and 7c.

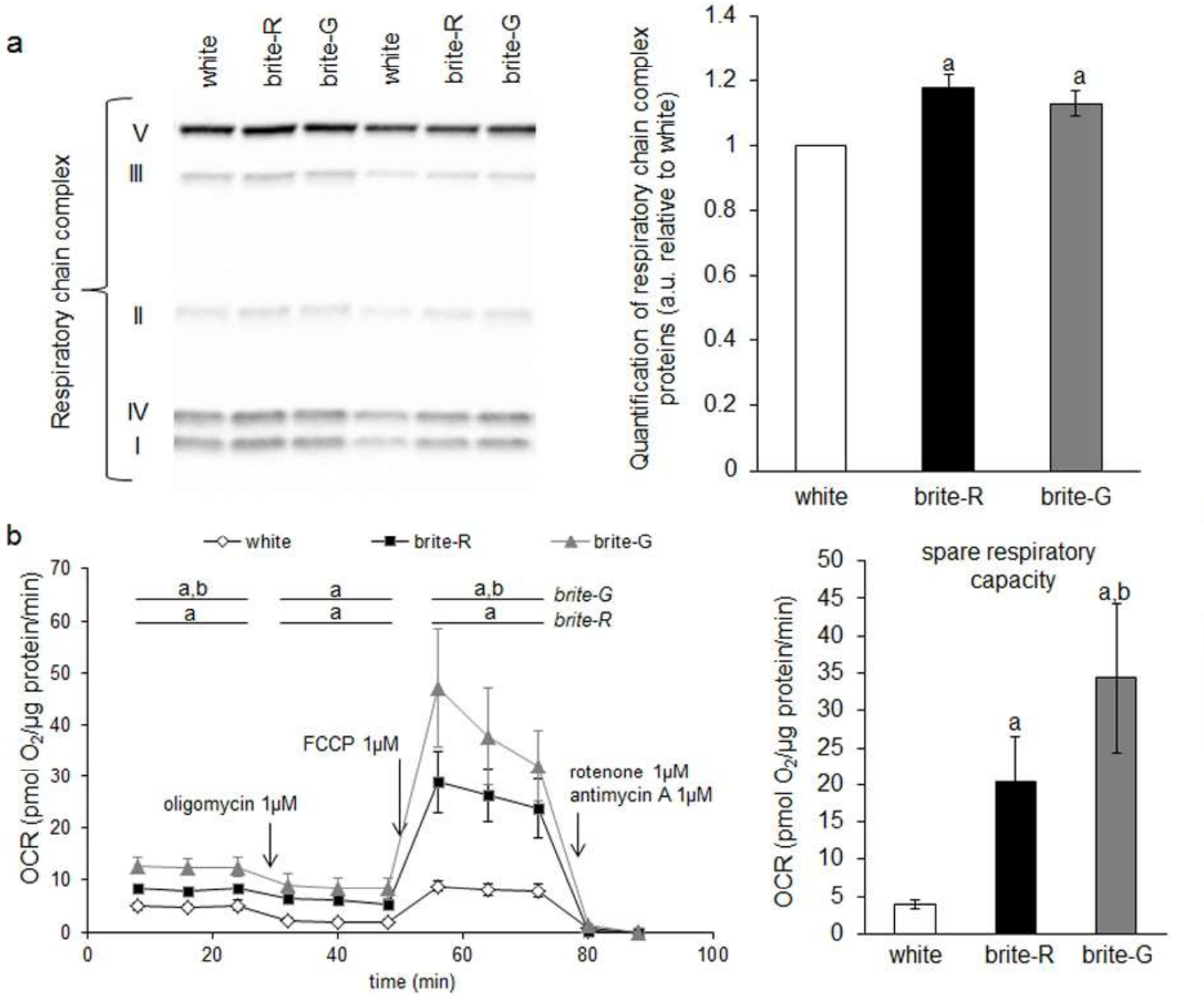
a
white
brite-R
brite-G
white
brite-R
brite-G
Respiratory chain complex
V
III
II
IV
I
Quantification of respiratory chain complex proteins (a.u. relative to white)
1.4
1.2
1
0.8
0.6
0.4
0.2
0
a
a
white
brite-R
brite-G
b
white
brite-R
brite-G
OCR (pmol O2/µg protein/min)
a,b
a
a
a
a,b
a
brite-G
brite-R
FCCP 1µM
oligomycin 1µM
rotenone 1µM
antimycin A 1µM
time (min)
spare respiratory capacity
a
a,b
white
brite-R
brite-G

white
brite-R
TIMM23
UCP1
TIMM23
UCP1
TIMM23
UCP1

a

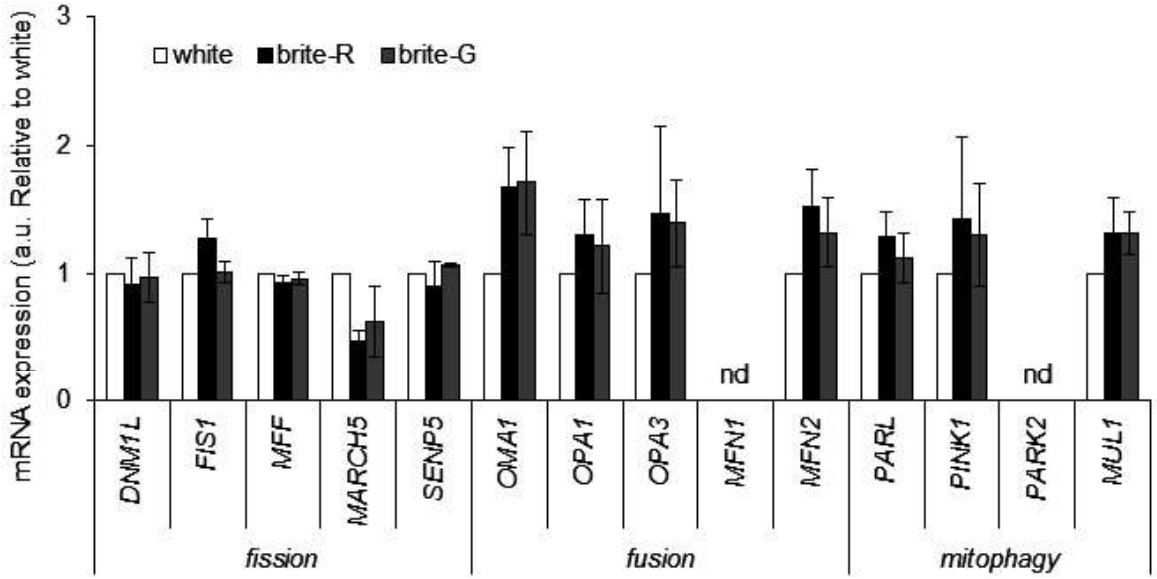
mRNA expression (a.u. Relative to white)
3
2
1
0
white
brite-R
brite-G
nd
nd
DNM1L
FIS1
MFF
MARCH5
SENP5
OMA1
OPA1
OPA3
MFN1
MFN2
PARL
PINK1
PARK2
MUL1
fission
fusion
mitophagy

b

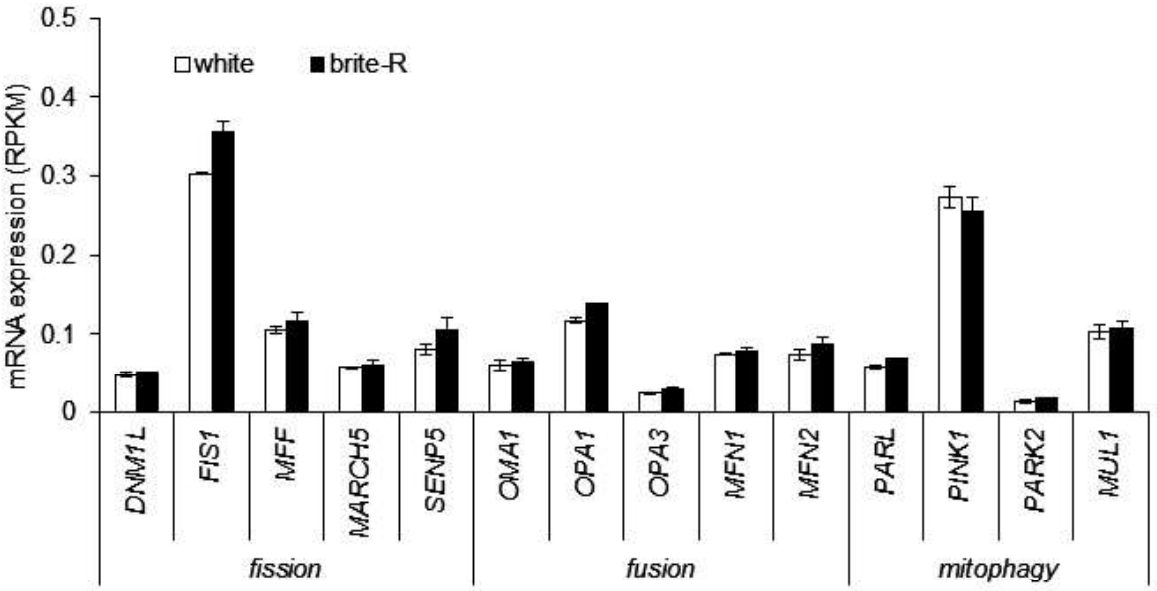
mRNA expression (RPKM)
0.5
0.4
0.3
0.2
0.1
0
white
brite-R
DNM1L
FIS1
MFF
MARCH5
SENP5
OMA1
OPA1
OPA3
MFN1
MFN2
PARL
PINK1
PARK2
MUL1
fission
fusion
mitophagy

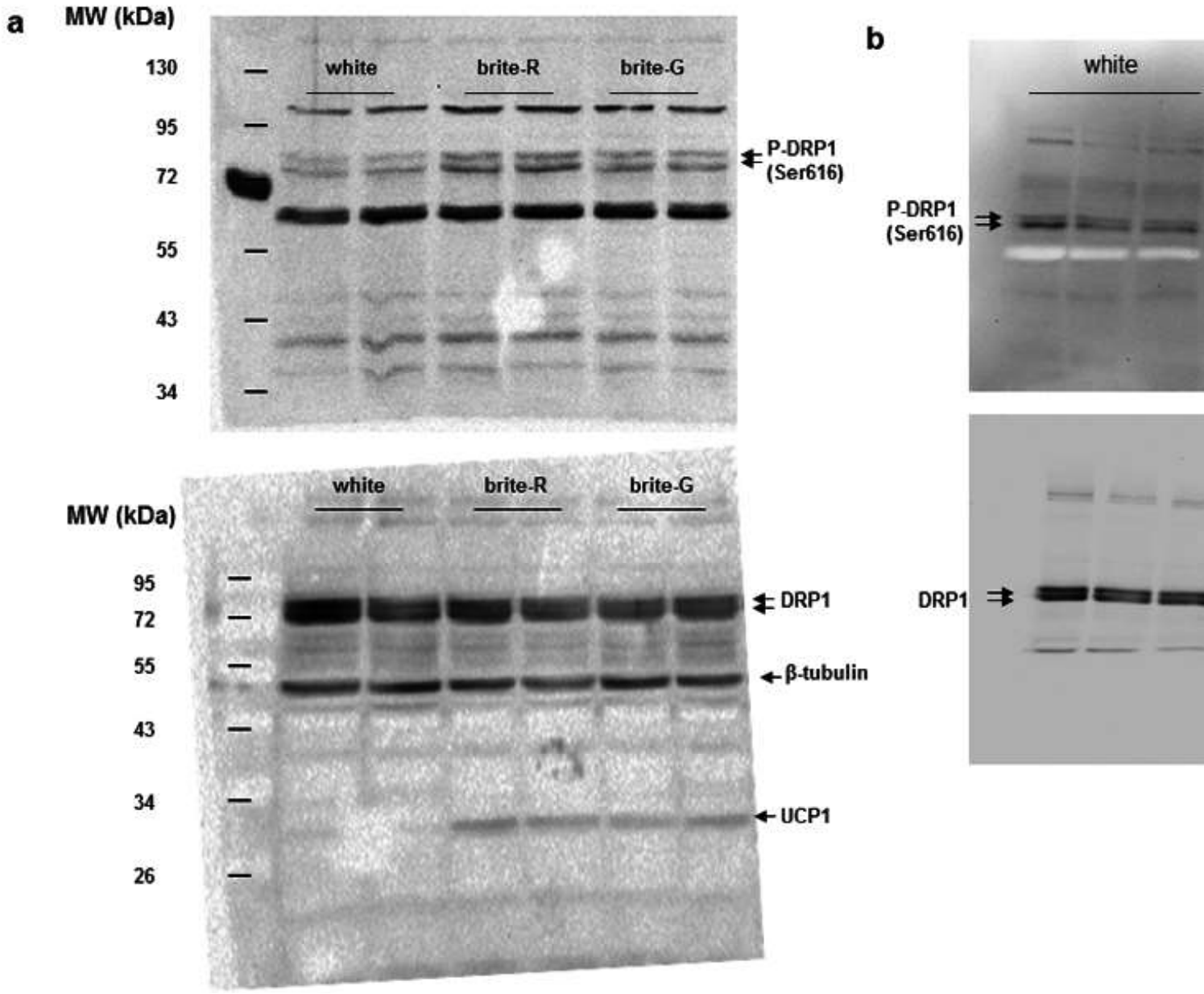
a
MW (kDa)
130
95
72
55
43
34
white
brite-R
brite-G
P-DRP1
(Ser616)
MW (kDa)
95
72
55
43
34
26
white
brite-R
brite-G
DRP1
β-tubulin
UCP1
b
white
P-DRP1
(Ser616)
DRP1

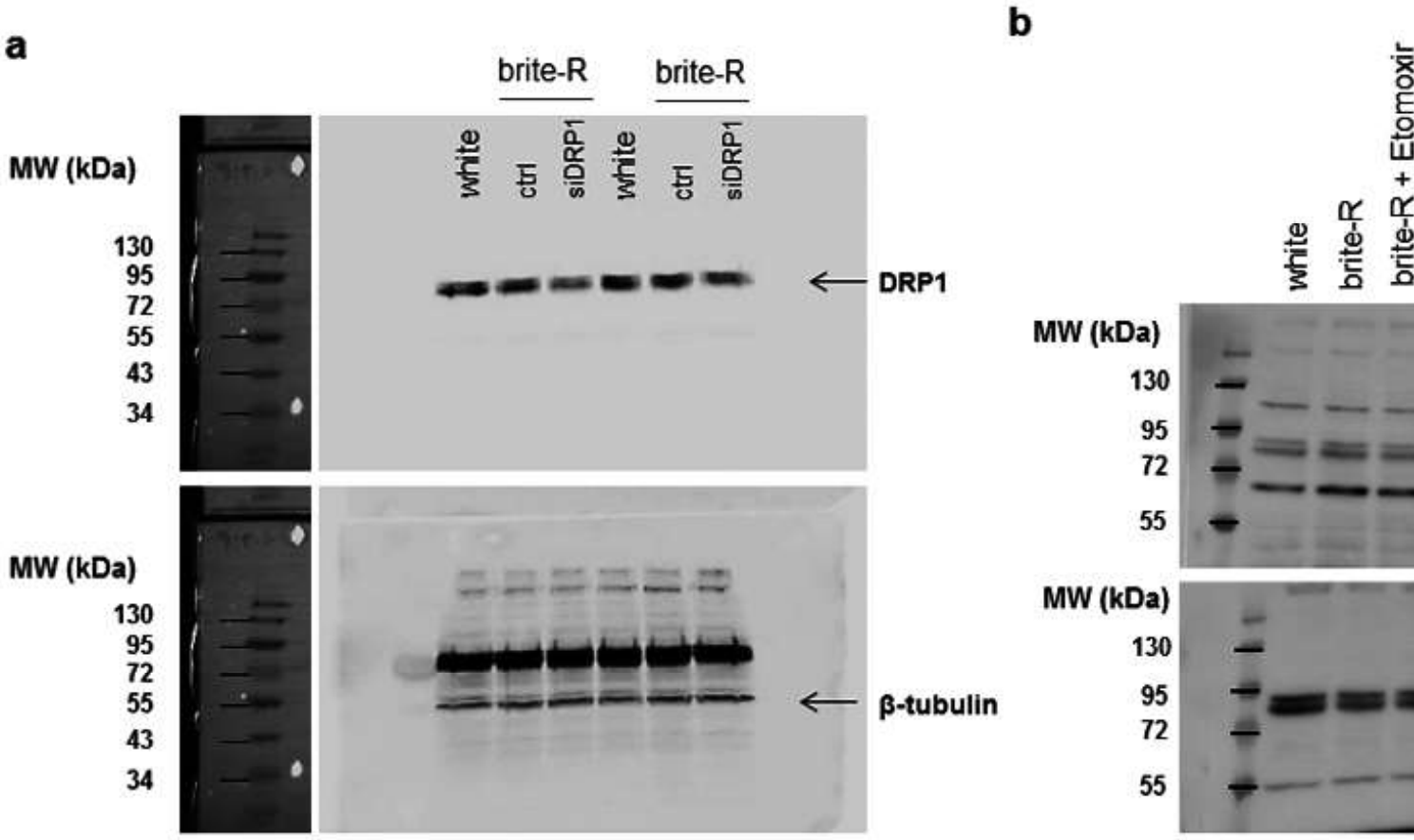
a
brite-R
brite-R
white
ctrl
siDRP1
white
ctrl
siDRP1
MW (kDa)
130
95
72
55
43
34
DRP1
MW (kDa)
130
95
72
55
43
34
β-tubulin
b
white
brite-R
brite-R + Etomoxir
MW (kDa)
130
95
72
55
MW (kDa)
130
95
72
55

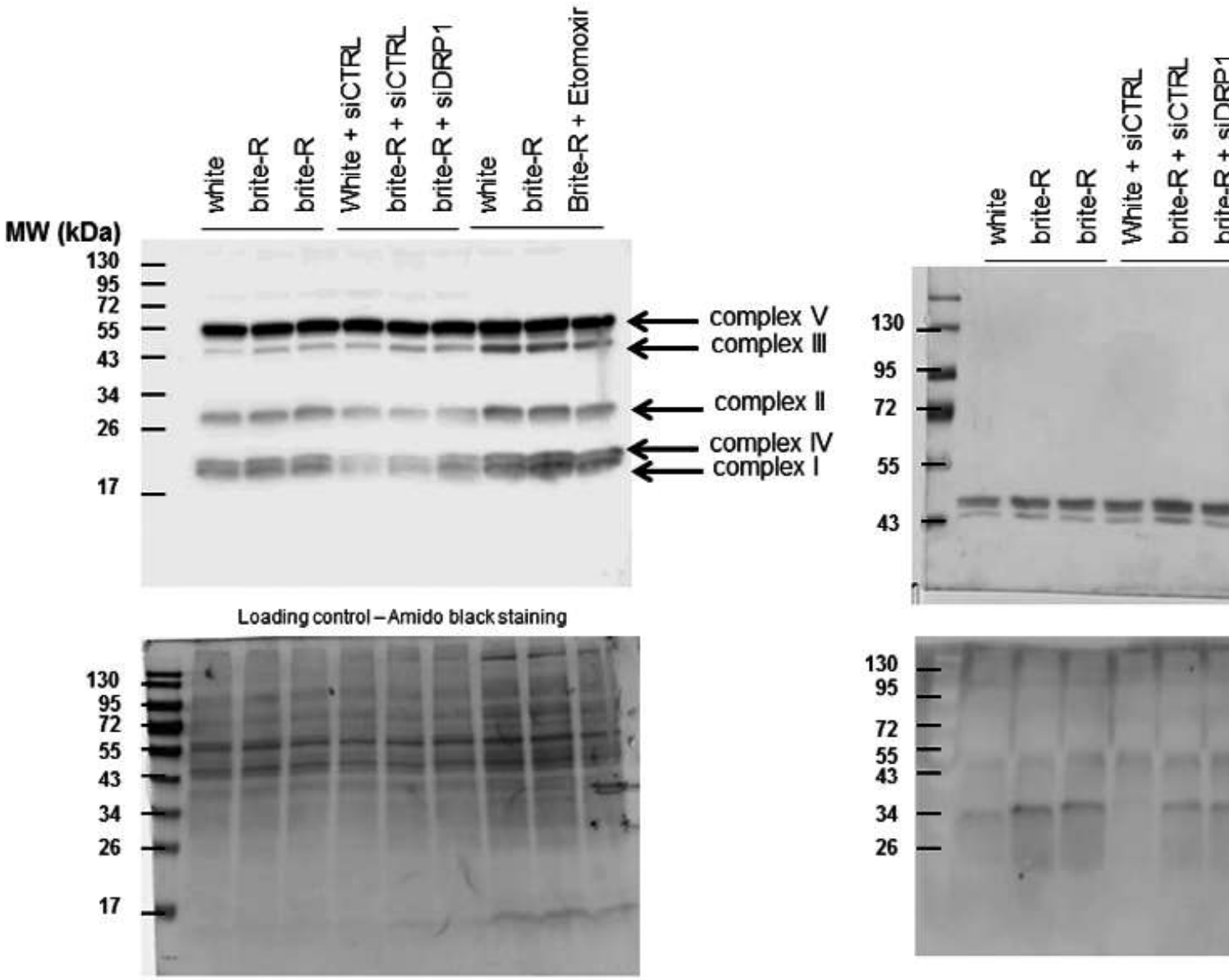
white
brite-R
brite-R
White + siCTRL
brite-R + siCTRL
brite-R + siDRP1
white
brite-R
Brite-R + Etomoxir
MW (kDa)
130
95
72
55
43
34
26
17
complex V
complex III
complex II
complex IV
complex I
Loading control – Amido black staining
white
brite-R
brite-R
White + siCTRL
brite-R + siCTRL
130
95
72
55
43
130
95
72
55
43
34
26
17
130
95
72
55
43
34
26